# Empirical formulas for calculating loss in hollow core tube lattice fibers

**Luca Vincetti**[*]

*Department of Engineering "Enzo Ferrari" University of Modena and Reggio Emilia, 41125 Modena, Italy*
[*]*luca.vincetti@unimore.it*

**Abstract:** In this paper scaling laws governing loss in hollow core tube lattice fibers are numerically investigated and discussed. Moreover, by starting from the analysis of the obtained numerical results, empirical formulas for the estimation of the minimum values of confinement loss, absorption loss, and surface scattering loss inside the transmission band are obtained. The proposed formulas show a good accuracy for fibers designed for applications ranging from THz to ultra violet band.

## References and links

1. V. Setti, L. Vincetti, and A. Argyros, "Flexible tube lattice fibers for terahertz applications," Opt. Express **21**(3), 3388–3399 (2013).
2. W. Lu and A. Argyros, "Terahertz spectroscopy and imaging with flexible tube-lattice fiber probe," J. Lightwave Technol. **29**, 4621–4627 (2014).
3. A. D. Pryamikov, A. S. Biriukov, A. F. Kosolapov, V. G. Plotnichenko, S. L. Semjonov, and E. M. Dianov, "Demonstration of a waveguide regime for a silica hollow - core microstructured optical fiber with a negative curvature of the core boundary in the spectral region > 3.5 μm," Opt. Express **19**(2), 1441–1448 (2011).
4. A. F. Kosolapov, A. D. Pryamikov, A. S. Biriukov, V. S. Shiryaev, M. S. Astapovich, G. E. Snopatin, V. G. Plotnichenko, M. F. Churbanov, and E. M. Dianov, "Demonstration of CO2-laser power delivery through chalcogenide-glass fiber with negative-curvature hollow core," Opt. Express **19**(25), 25723–25728 (2011).
5. A. N. Kolyadin, A. F. Kosolapov, A. D. Pryamikov, A. S. Biriukov, V. G. Plotnichenko, and E. M. Dianov, "Light transmission in negative curvature hollow core fiber in extremely high material loss region," Opt. Express **21**(8), 9514–9519 (2013).
6. W. Belardi and J. C. Knight, "Hollow antiresonant fibers with low bending loss," Opt. Express **22**(8), 10091–10096 (2014).
7. F. Couny, F. Benabid, P. J. Roberts, P. S. Light, and M. G. Raymer, "Generation and photonic guidance of multi-octave optical-frequency combs," Science **318**(5853), 1118–1121 (2007).
8. B. Debord, M. Alharbi, T. Bradley, C. Fourcade-Dutin, Y. Y. Wang, L. Vincetti, F. Gérôme, and F. Benabid, "Hypocycloid-shaped hollow-core photonic crystal fiber Part I: arc curvature effect on confinement loss," Opt. Express **21**(23), 28597–28608 (2013).
9. B. Debord, A. Amsanpally, M. Alharbi, L. Vincetti, J. Blondy, F. Gérôme, and F. Benabid, "Ultra-large core size hypocycloid-shape inhibited coupling kagome fibers for high-energy laser beam handling," J. Lightwave Technol. **33**(17), 3630–3634 (2015).
10. A. Urich, R. R. Maier, F. Yu, J. C. Knight, D. P. Hand, and J. D. Shephard, "Flexible delivery of Er:YAG radiation at 2.94 μm with negative curvature silica glass fibers: a new solution for minimally invasive surgical procedures," Biomed. Opt. Express **4**(2), 193–205 (2013).
11. B. Debord, M. Alharbi, L. Vincetti, A. Husakou, C. Fourcade-Dutin, C. Hoenninger, E. Mottay, F. Gérôme, and F. Benabid, "Multi-meter fiber-delivery and pulse self-compression of milli-Joule femtosecond laser and fiber-aided laser-micromachining," Opt. Express **22**(9), 10735–10746 (2014).
12. P. Jaworski, F. Yu, R. R. Maier, W. J. Wadsworth, J. C. Knight, J. D. Shephard, and D. P. Hand, "Picosecond and nanosecond pulse delivery through a hollow-core Negative Curvature Fiber for micro-machining applications," Opt. Express **21**(19), 22742–22753 (2013).
13. P. J. Roberts, F. Couny, H. Sabert, B. J. Mangan, D. P. Williams, L. Farr, M. W. Mason, A. Tomlinson, T. A. Birks, J. C. Knight, and P. St. J. Russell, "Ultimate low loss of hollow-core photonic crystal fibres," Opt. Express **13**(1), 236-244 (2005).
14. E. N. Fokoua, F. Poletti, and D. J. Richardson, "Analysis of light scattering from surface roughness in hollow-core photonic bandgap fibers," Opt. Express **20**(19), 20980–20991 (2012).
15. E. N. Fokoua, S. R. Sandoghchi, Y. Chen, G. T. Jasion, N. V. Wheeler, N. K. Baddela, J. R. Hayes, M. N. Petrovich, D. J. Richardson, and F. Poletti, "Accurate modelling of fabricated hollow-core photonic bandgap fibers," Opt. Express **23**(18), 23117–23132 (2015).
16. F. Poletti, "Nested antiresonant nodeless hollow core fiber," Opt. Express **22**(20), 23807–23828 (2014).

17. S. Selleri, L. Vincetti, A. Cucinotta, and M. Zoboli, "Complex FEM modal solver of optical waveguides with PML boundary conditions," Opt. Quantum Electron. **33**(4), 359–371 (2001).
18. L. Vincetti and V. Setti, "Waveguiding mechanism in tube lattice fibers," Opt. Express **18**(22), 23133–23146 (2010).
19. L. Vincetti, V. Setti, and M. Zoboli, "Terahertz tube lattice fibers with octagonal symmetry," IEEE Photonics Technol. Lett. **22**(13), 972–974 (2010).
20. M. Kharadly and J. Lewis, "Properties of dielectric-tube waveguides," Proc. IEEE **116**, 214–224 (1969).
21. G. K. Alagashev, A. D. Pryamikov, A. F. Kosolapov, A. N. Kolyadin, A. Y. Lukovkin, and A. S. Biriukov, "Impact of geometrical parameters on the optical properties of negative curvature hollow-core fibers," Laser Phys. **25**(5), 055101 (2015).
22. M. Masruri, A. Cucinotta, and L. Vincetti, "Scaling laws in tube lattice fibers," in *CLEO: 2015*, OSA Technical Digest (online) (Optical Society of America, 2015), paper STu1N.8.
23. E. A. Marcatili and R. A. Schmeltzer, "Hollow metallic and dielectric waveguides for long distance optical transmission and lasers," Bell Syst. Tech. J. **43**(4), 1783–1809 (1964).
24. D. S. Wu, A. Argyros, and S. G. Leon-Saval, "Reducing the size of hollow terahertz waveguides," J. Lightwave Technol. **29**(1), 97–103 (2011).

## 1. Introduction

Hollow core - Tube lattice fibers (HC-TLFs) also called anti-resonant fibers, with negative curvature, are more and more diffused fiber for applications ranging from THz to infrared [1–6]. Terahertz imaging [2], high power beam delivering in medium infrared spectral region [4], low loss transmission by using highly absorbing materials [1, 5], are just some application examples of this kind of fibers characterized by a quite simple cross section and very interesting transmission properties. HC-TLFs consist of a ring of dielectric tubes surrounding a hollow core. The waveguiding mechanism is the same of the Kagome Fibers, that is the inhibition of the coupling of the cladding and core modes [7, 8]. Inhibited coupling (IC) fibers suffer of three different loss mechanisms: the confinement loss (CL), the material absorption, and the surface scattering loss (SSL). The former, related to the leaky nature of the modes, is dominant in the near infrared spectral region where low loss silica is often used as dielectric material [8]. Conversely in the far infrared and terahertz regions, dielectrics exhibit much higher loss making dominant the absorption loss [1, 5], even though the extremely low field dielectric overlap (DO) allows to dramatically reduce the absorption loss (AL) with respect to other kind of waveguides [1]. In addition, the low DO also allows to significantly increase the Laser Induced Damage Threshold (LIDT) [9, 10]. High power beam delivery has been recently demonstrated in HC-IC fibers in the near infrared region [11,12]. Finally, SSL is due to the surface roughness of the air-dielectric interface [13–16]. Its analysis requires the knowledge of the roughness power spectral density which is quite hard to measure. However, SSL can be efficiently estimated by considering the electric field on interface (EI) between air and dielectric [13, 15, 16].

In HC-TLFs CL, DO, and EI depend on the interaction among the core and the cladding modes, which in turn depends on plenty of fibers' parameters such as core size, number and size of the tubes, dielectric refractive index, and wavelength. The lack of analytical models able to quantify CL, DO, and EI obligates to analyze such kind of fibers by using numerical approaches, making hard their design, and optimization. Scaling laws and analytical formulas relating fiber parameters and loss can help both the design and the optimization of HC-TLFs as well as to improve the physical insight into their guidance mechanism. In this work the dependence of CL, DO and EI of the fiber's fundamental mode (FM) on the wavelength, core size and cladding parameters are numerically analyzed by considering several HC-TLFs working in completely different spectral ranges from terahertz (THz) to ultraviolet (UV) and composed by different materials. The numerical results have been obtained through the modal solver of the commercial software Comsol Multiphysics 3.5 based on the finite-element method, with an optimized anisotropic perfectly matched layer (PML) [17]. By starting from all those numerical data, through both fitting techniques and working hypothesis based on knowledge of waveguiding mechanism in HC-TLFs, analytical formulas for CL, AL and SSL of the FM are empirically obtained. The formulas use as input data only the parameters of the tubes composing the cladding (refractive index, number, size and thickness). Results show a good accuracy of the formulas despite most of the parameters range over several decades.

## 2. Fiber Geometry, guiding mechanism, loss and single tube model

HC-TLFs are fibers composed by a regular arrangement of $N$ dielectric tubes surrounding the hollow core [18]. An example of cross section with $N = 8$ is shown in Fig. 1(a). The tubes have outer radius $r_{ext}$, dielectric thickness $t$, and refractive index $n_d$. They can touch each other ($\delta = 0$) [1–4] or not ($\delta > 0$) [5, 6]. For all the simulated fibers here considered, tubes penetrate into the surrounding dielectric of $t/100$. The core size depends on number, size, and distance between the tubes:

$$R_{co} = \left[ \left( k \Big/ \sin(\frac{\pi}{N}) \right) - 1 \right] r_{ext}, \qquad (1)$$

being: $k = 1 + \delta/(2r_{ext})$.

In the next subsections the guiding mechanism of HC-TLFs and the single tube model (STM) [18] are briefly reviewed to highlight the main concepts used in the following sections.

### 2.1 Guiding mechanism

In HC-TLFs the waveguide mechanism is the same of Kagome Fibers and it is based on the inhibition of the coupling between the core and the cladding modes [7]. Strong coupling between two modes can occur at the resonance condition ($n_{eff_1} \square n_{eff_2}$) if the overlap integral $\int_{S_\infty} \vec{E}_1 \cdot \vec{E}_2 dS$ is not negligible, being $n_{eff}$ and $\vec{E}$ the effective index and the electric field of the modes respectively.
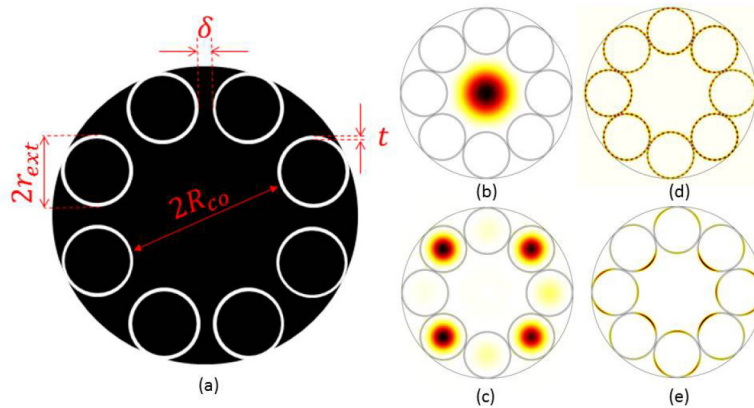


Fig. 1. (a) Cross section of a HC-TLF with non-touching tubes and $N = 8$. Black is air with unitary refractive index and white the dielectric with refractive index $n_d$; (b) fundamental core mode. (c) holes cladding mode; (d)-(e) dielectric cladding modes with fast and slow spatial oscillation respectively.

HC-TLFs support three different kinds of modes shown in Figs. 1(b)-1(e): The core modes (CMs) (Fig. 1(b)) with the power mainly confined inside the hollow core; the hole cladding modes (or airy modes) (HCMs) confined inside the holes of the tubes (Fig. 1(c)); the dielectric cladding modes (DCMs) mainly confined inside the dielectric (Figs. 1(d) and 1(e)).

In the confinement mechanism of the CMs, DCMs are mainly involved. Since DCMs are confined in the dielectric and CMs in the air, resonance condition can only occur at cut-off frequencies of the former ones. In addition the overlap integral is not negligible only with DCMs having slow spatial dependence [7]. As a consequence, CMs suffer of high loss in the spectral ranges where there are cut-off frequencies of DCMs with slow spatial oscillations.

On the contrary the coupling and thus the loss are low in the spectral regions where there are only cut-off frequencies of DCMs with fast spatial oscillations.

By restricting the analysis to HC-TLFs with $N > 7$, the FM effective index is always higher than the HM ones and thus the resonance condition is never satisfied. Under these conditions HMs do not significantly affect the propagation of the FM. Nevertheless, they can be used to enhance the loss of high order CMs improving the single-modeness condition [18, 19], and to explain resonances in HC-TLF bending loss [1].

### 2.2 Loss in HC-TLFs

In HC-TLFs the propagation loss is mainly caused by the leaky nature of the CMs, by the dielectric absorption, and by the scattering due to the dielectric surface roughness.

Confinement loss can be estimated by considering the confinement loss parameter:

$$CL(\lambda) = 8.686 \, \text{Im}[\gamma(\lambda)] \ [dB/m],$$

being $\gamma$ the complex eigenvector of the mode.

The absorption loss can be estimated by considering the following coefficient:

$$AL(\lambda) = \alpha_d(\lambda) DO(\lambda),$$

where $\alpha_d$ is the absorption coefficient of the dielectric composing the cladding, and DO the dielectric overlap parameter:

$$DO(\lambda) = \int_{s_d} p_z dS \left/ \int_{s_\infty} p_z dS \right. ,$$

being $S_\infty$, $S_d$, and $p_z$ the whole fiber cross section, the cross section occupied by the dielectric, and the longitudinal component of the FM Poynting vector respectively.

The estimation of SSL is more complex, because it would require a statistical treatment of the scattering process which requires an accurate knowledge of the surface roughness spectral density. Since in practice it is hard to measure such kind of quantity, a simplified but effective approach is here used. SSL is estimated by mean of the following formula [16]:

$$SSL_{\min}(\lambda) = \eta EI(\lambda) \left(\frac{\lambda_0}{\lambda}\right)^3,$$

where $\eta$ and $\lambda_0$ are two coefficients depending of the roughness, and $EI$ is the electric field at the interface parameter [13]:

$$EI = \sqrt{\frac{\varepsilon_0}{\mu_0}} \oint_{l_d} |\vec{E}|^2 \, dl \left/ \int_{S_\infty} p_z dS \right. ,$$

being $l_d$ the air-dielectric interface, and $\vec{E}$ the FM electric field.

Due to the high absorption coefficient of the dielectrics, in THz and mid-infrared (MIR) spectral regions, $AL$ is often dominant with respect to the other two mechanisms [1, 5, 6]. In the near infrared region (NIR), the extremely low absorption coefficient of the silica makes dominant the confinement loss; at very short wavelengths (visible and ultraviolet – VUV) SSL can play a significant role [16].

### 2.3 Single tube model

In the single tube model, the DCMs of HC-TLFs are described as superposition of dielectric modes of a single Tube Fiber (TF) [18], and their cut-off frequencies estimated by the cut-off frequencies of the dielectric modes of a single TF. Figure 2 shows some examples of TF dielectric modes with different azimuthal and radial numbers $\mu$, and $\nu$ respectively. Figure 2

also shows the cut-off frequencies of the dielectric modes with the slowest azimuthal dependence. F is the normalized frequency [20]:

$$F = \frac{2t}{\lambda}\sqrt{n^2 - 1}. \tag{2}$$

For a given mode, the cut-off frequency depends on the parameter $\rho = 1 - t/r_{ext}$ and on the dielectric refractive index $n_d$ of the tube. The modes with the lowest azimuthal dependence and thus the strongest coupling with CMs are the $HE_{v,1}$. Figure 2 shows that their cut-off frequencies (green empty circles) are very close to the values $F = v{-}1 = m$, with $m$ integer, that results in the condition $\lambda_m = 2t/m\sqrt{n^2 - 1}$ often used to estimate the spectral position of high loss regions in IC fibers. Actually this condition is an asymptotic condition true when $\rho \rightarrow 1$.

As $\rho$ approaches 1, all cut-off frequencies get closer and closer to $F = v{-}1 = m$. Conversely, for low $\rho$ values and/or high $n_d$ the cut-off frequencies of the modes with slow spatial oscillations broaden resulting in wider high loss regions. This is confirmed by Fig. 3 where $CL$ and $DO$ spectra of four HC-TLFs with different $\rho$ and $n_d$ are shown. The high loss regions extend further the condition $F = v{-}1$ due to the coupling with DCMs with $\mu > 1$. A numerical evidence of such coupling is reported in [21]. Moreover, the fibers with lower $\rho$ or higher $n_d$ exhibit wider high value spectral regions. The same trend, not shown here for sake of brevity, is observed for $EI$. Due to that, the loss minima do not fall in the middle of a transmission band but are shifted toward higher frequencies.
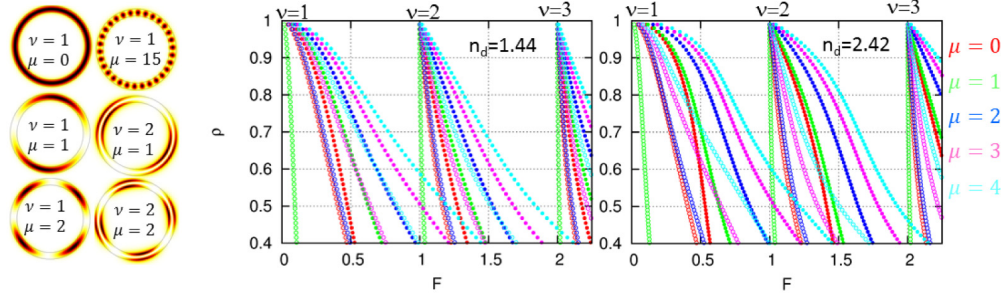


Fig. 2. Left: Examples of the electric field modulus distribution of some dielectric modes of a single tube fiber. Right: Normalized cut-off frequencies versus $\rho$ parameter, for two different dielectric refractive indices: $n_d = 1.44, 2.42$. Different colors show curves of modes with different azimuthal number $\mu$ from $0$ to $4$. Empty and filled circles refer to HE and EH modes respectively.

From this brief discussion it is clear that in HC-TLFs, $CL$, $DO$, and $EI$ depend on cut-off frequency distribution of DCMs in addition to core size, and wavelength. By using STM, that dependence can be led back to $t$, $r_{ext}$, $N$, $n_d$ of the tubes composing the cladding. In the next sections the $CL$, $DO$, and $EI$ dependences of the FM on tubes' parameters will be investigated.
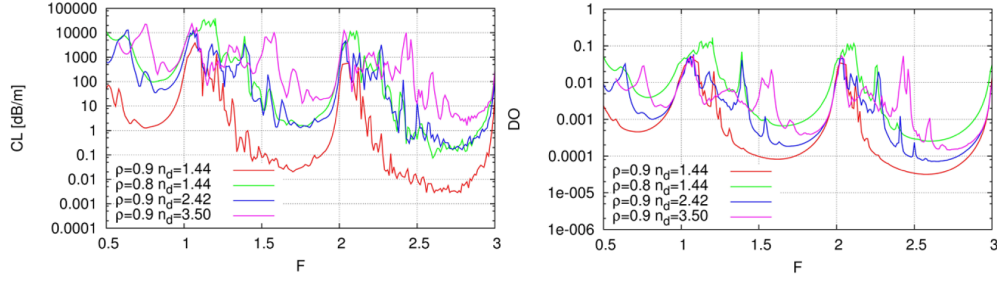
Fig. 3. Confinement loss (left) and dielectric overlap (right) of four fibers with $t = 1um$, $N = 8$, $\delta = 0$, and different values of $\rho$ and $n_d$.

## 3. Analysis of the CL dependences

The analysis of the effects of the above mentioned parameters is made complex because it is hard to separate the effect of one from the others. For example by changing the tube thickness $t$ both the $\rho$ parameter and the working wavelength are changed, or by changing the tubes radius $r_{ext}$, both $R_{co}$ and $\rho$ are changed. In order to unravel all the dependences, several fiber with completely different cladding parameters have been investigated. Table 1 summarizes the fibers and their parameters considered in the analysis. The tube thickness ranges from fractions to hundreds of micrometers, corresponding to fibers working in the UV and THz bands respectively. $n_d = 1.44$, $2.42$, $1.521$ corresponds to the refractive index of the silica in the NIR, of the chalcogenide glass in the MIR, and of the Zeonex in THz regions. Other values of $n_d$ have been chosen to better analyze the dependences on the parameters and they are gathered in the set MIS in Tab. 1. The number of tubes ranges from 8 to 20. Values lower than 8 have not been considered as with $k = 1$, FM propagation starts to be affected by resonances with the HCMs [22].

**Table 1. Sets of fibers considered in the analysis.**

| name | $t[um]$ | $r_{ext}[um]$ | $\delta\ [um]$ | $n_d$ | $N$ | $R_{co}[um]$ | $\rho$ |
|---|---|---|---|---|---|---|---|
| VUV | 0.2 | 1 ÷ 5 | 0 | 1.500 | 8 ÷ 28 | 8um | 0.80 ÷ 0.96 |
| NIR | 0.5 | 5 | 0 ÷ 3 | 1.440 | 8 ÷ 14 | 8um ÷ 14um | 0.9 |
| MIR | 1.0 | 10 | 0 | 2.420 | 8 ÷ 14 | 16um ÷ 35um | 0.9 |
| THz | 131 | 1746 | 0 ÷ 393 | 1.521 | 8 ÷ 20 | 2.8mm ÷ 9.4mm | 0.925 |
| MIS | 0.495 ÷ 1.26 | 6.18 ÷ 15.81 | 0 | 1.441 ÷ 2.8355 | 8-16 | 25.5um | 0.92 |

### 3.1 Wavelength and core size dependence

Wavelength and core size dependences have been recently numerically investigated by considering several HC-TLFs composed by Zeonex tubes for THz transmission [22]. Here the analysis is extended by considering additional fibers working in other spectral ranges. In order to investigate the core size dependence without changing the other cladding parameters, several fibers having same tubes but in a different number $N$ have been considered. The core radius $R_{co}$ changes according to Eq. (1).
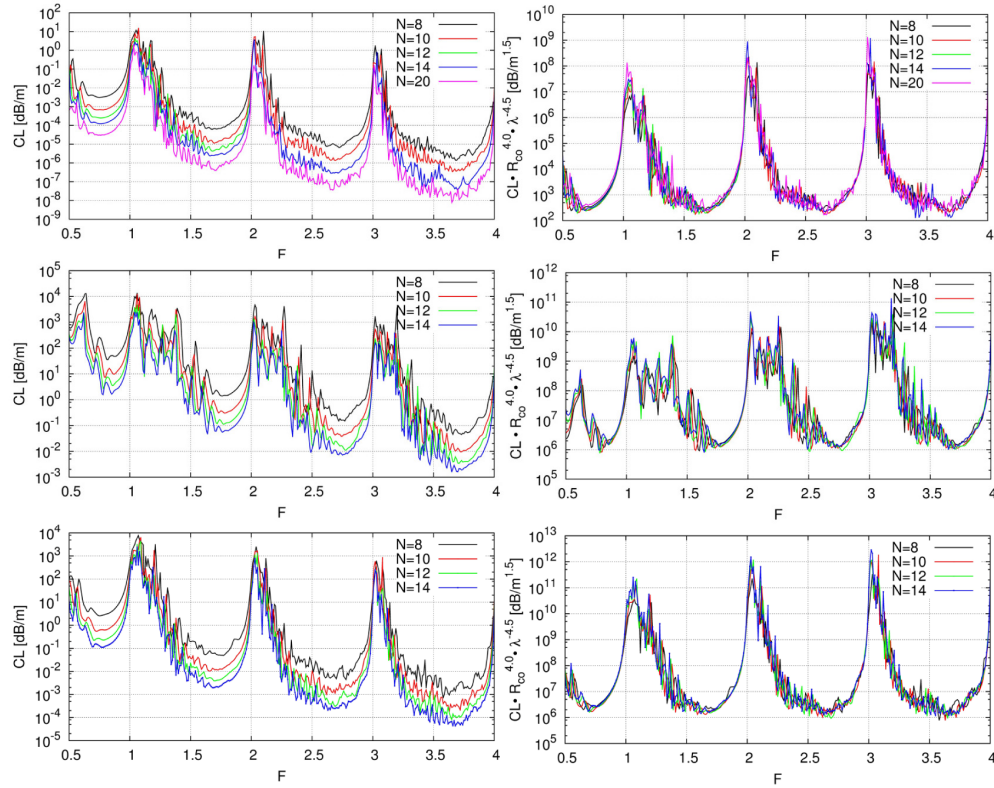
Fig. 4. *CL* (left column) and *CL* $R_{co}^4/\lambda^{4.5}$ (right column) of fibers THz with $t = 131um$, $r_{ext} = 1746um$, $n_d = 1.521$ (top), MIR with $t = 1.0um$, $r_{ext} = 10um$, $n_d = 2.42$ (middle), and NIR with $t = 0.5um$, $r_{ext} = 5um$, $n_d = 1.44$ (bottom) having different number of tubes *N* and thus different $R_{co}$. All fibers have $\delta = 0$.

Figure 4 compares *CL* with the normalized parameter $CL \cdot R_{co}^4/\lambda^{4.5}$ of different sets of fibers: THz, MIR, and NIR. Despite *CL* ranges over decades by changing $R_{co}$ and λ, now the normalized curves are almost overlapped and the minima no longer depend on core size and wavelength. Other results, not shown here for the sake of brevity, confirm that *CL* scales as $\lambda^{4.5}/R_{co}^4$ irrespectively on working wavelength range and size of the fiber.

### 3.2 ρ parameter dependence

According to STM, by changing *ρ*, the DCMs cut-off map changes affecting the *CL*. To investigate that dependence some HC-TLFs with same tube thickness (and thus same working wavelength) and same core size have been considered. $r_{ext}$ and *N* have been changed in order to have $R_{co} = 8um$.
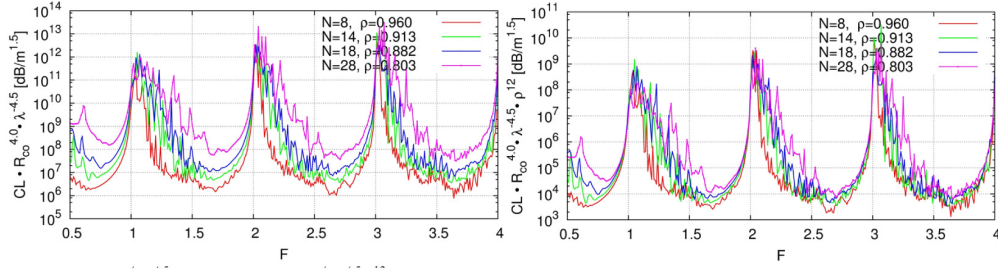
Fig. 5. $CL \, R_{co}^4/\lambda^{4.5}$ (left) and $CL \, R_{co}^4/\lambda^{4.5}\rho^{12}$ (right) of fibers VUV having different $\rho$ parameter, different number of tubes $N$, and $R_{co} = 8um$, $t = 0.2um$, $n_d = 1.5$. All fibers have $\delta = 0$.

Despite the core size and working wavelength are the same for all fibers, Fig. 5 shows that $CL$ increases as $\rho$ reduces. The broadening of high loss regions is due to the shift of the DCM cut-off frequencies described in the section 3. By analyzing the spectra, it results that the minima of CL are proportional to $1/\rho^{12}$. This is confirmed by the normalized coefficient $CL \, R_{co}^4/\lambda^{4.5}\rho^{12}$ spectra shown in Fig. 5. The minima of the different fibers curves are now closer and it is clearer the broadening of the high loss regions related to lower $\rho$ values. Same results have been obtained for fiber working in THz, MIR, and NIR ranges. Notice that a dependence on the 12th power can seem a huge dependence. Actually it is not so strong because $\rho$ is a normalized parameter. It usually ranges from $0.8$ to $0.97$, and this corresponds to a $\rho^{12}$ ranging from $0.07$ to $0.7$, that is a decade.

### 3.3 Refractive index dependence

According to the STM, the cladding modes cut-off do not only depend on the $\rho$ parameter, they also depend on the refractive index $n_d$ and this results in a $CL$ dependence on dielectric refractive index.
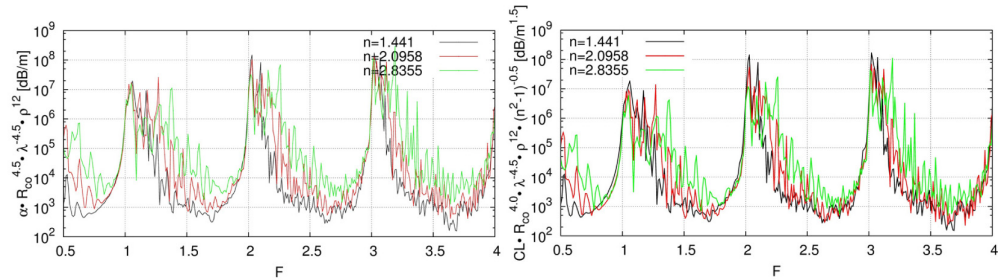


Fig. 6. $CL \, R_{co}^4/\lambda^{4.5}\rho^{12}$ (left) and $CL \, R_{co}^4 \big/ \lambda^{4.5} \cdot \rho^{12} \big/ \sqrt{n^2-1}$ (right) of MIS fibers having different $n_d$ and $t$. All fibers have $\delta = 0$, $R_{co} = 25.5um$, and $\rho = 0.92$.

In order to highlight this dependence, Fig. 6(a) shows the spectra of the coefficient $CL \, R_{co}^4/\lambda^{4.5}\rho^{12}$ of different fibers with three different refractive index values: 1.441, 2.0958, 2.8355. $t$ also changes in order to have the same $t\sqrt{n^2-1}$ product and thus same working wavelength. Also $r_{ext}$ changes to have $\rho = 0.92$. $CL$ increases with $n_d$ due to the cladding mode cut-off frequencies spreading. It is estimated that $CL$ is proportional to $\sqrt{n^2-1}$. This is confirmed by the overlapping of the minima of the coefficient $CL \, R_{co}^4 \big/ \lambda^{4.5} \cdot \rho^{12} \big/ \sqrt{n^2-1}$ spectra shown in Fig. 6(b). Again, the normalization more clearly shows the spectral broadening of the high loss regions due to the higher refractive index. This is also shown in Fig. 4 since chalcogenide glass (middle) has higher refractive index than the other materials considered (top and bottom).

## 3.4 Additional dependences

There are also additional dependences which are apparent only if the involved parameters change over wide ranges. Figure 7(a) shows the spectra of the VUV, NIR, MIR, and THz fibers. The confinement loss ranges over 10 decades. In Fig. 7(b) the spectra of $CL\,R_{co}^{\;4}/\lambda^{4.5}\cdot\rho^{12}/\sqrt{n^2-1}$ of VUV, NIR, MIR, and THz fibers are shown.
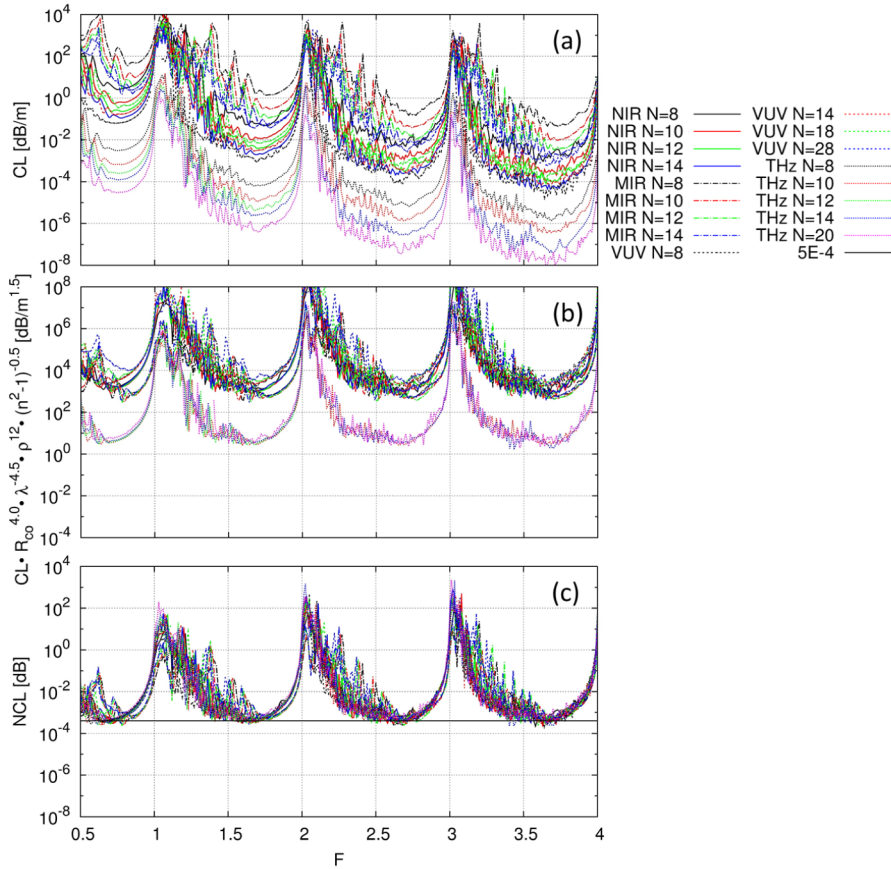


Fig. 7. *CL* (a), $CL\,R_{co}^{\;4}/\lambda^{4.5}\cdot\rho^{12}/\sqrt{n^2-1}$ (b), and *NLC* (c) spectra of the fibers: VUV, NIR, MIR, and THz, described in the Table 1 with $\delta = 0$.

The gaps between the spectra of the different sets of fibers are due to the dependences till now disregarded. By taking into account those, the following normalized *CL* coefficient can be defined:

$$NCL = CL\,\frac{R_{co}^{\;4}}{\lambda^{4.5}}\,\frac{t\rho^{12}}{\sqrt{n^2-1}}\sqrt{\frac{r_{ext}}{\lambda}}\,e^{-2\frac{\lambda}{r_{ext}(n^2-1)}}.$$

Figure 7(c) shows the spectra of *NCL*. Notice that despite the huge variation of *CL* in Fig. 7(a) (about 10 decades), the minima in the *NCL* spectra are all very close each other. The main discrepancies are caused by the resonance peaks with cladding modes falling close to the *CL* minima in fibers with high refractive index and/or low $\rho$ parameter due to the spreading of the cut-off frequencies.
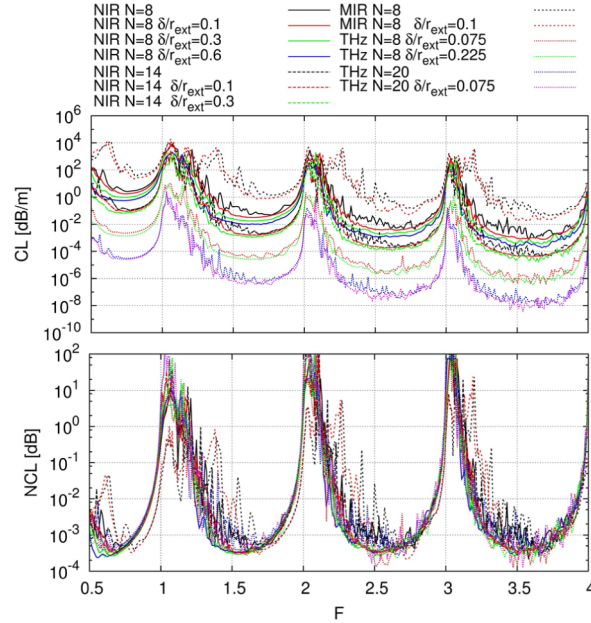
Fig. 8. *CL* (top), and *NCL* (bottom) of NIR and THz with different values of *N* and $\delta$.

The same analysis has been carried out by considering HC-TLFs with no-touching tubes [5, 6]. The results are shown in Fig. 8. The spectra are smoother than those referring to $\delta = 0$, because the gaps between the tubes reduce the coupling between the tubes modes cleaning up the spectral density of DCMs [5]. However the *NCL* spectra are still overlapped.

### 3.5 Empirical formula for CL

Even though variations over several decades have been considered, the results in Figs. 7 and 8 show that the minima of *NCL* do not depend on fiber's parameter. The peaks in the CL spectra make hard the estimation of the minima values. However all the minima are within the range $[3\cdot10^{-4}, 7\cdot10^{-4}]$. If an average value $NCL_{min} = 5\cdot10^{-4}$ *dB* is assumed, by using Eq. (1), (2), and (3), the $\rho$ expression, and $NCL_{min}$, the following empirical formula able to predict the minima of *CL* in the HC-TLFs transmission bands can be obtained:

$$
CL_{min} = 5\cdot10^{-4} \frac{\lambda^{4.5}}{R_{co}{}^4} \left(1 - \frac{t}{r_{ext}}\right)^{-12} \frac{\sqrt{n^2-1}}{t\sqrt{r_{ext}}} e^{\frac{2\lambda}{r_{ext}(n^2-1)}}
$$

$$
= 5\cdot10^{-4} \left(\frac{k}{\sin\left(\frac{\pi}{N}\right)} - 1\right)^{-4} \left(\frac{\lambda}{r_{ext}}\right)^{4.5} \left(1 - \frac{t}{r_{ext}}\right)^{-12} \frac{\sqrt{n^2-1}}{t} e^{\frac{2\lambda}{r_{ext}(n^2-1)}} \quad [dB/m]. \tag{3}
$$

The equation only requires number, refractive index and geometrical dimension of the tubes composing the cladding surround the hollow core.

## 4. Analysis of the *DO* dependences

The same analysis has been carried out to investigate the dielectric overlap dependences. Figure 9 compares the *DO* of all fibers here investigated with the normalized *DO*:

$$
NDO = DO \left[\left(k \Big/ \sin\left(\frac{\pi}{N}\right)\right) - 1\right]^{2.93} \left(\frac{r_{ext}}{t}\right)^{0.93} \left(\frac{r_{ext}}{\lambda}\right)^2 n.
$$

Again the overlap is very good except the peaks due to the resonances in fibers with high index and/or low $\rho$. All the minima are within the range *[0.2, 0.28]*, with an average value: $NDO_{min} = 0.24$. There is just a spectral shift of the minima toward higher frequencies for fibers with higher $n_d$.
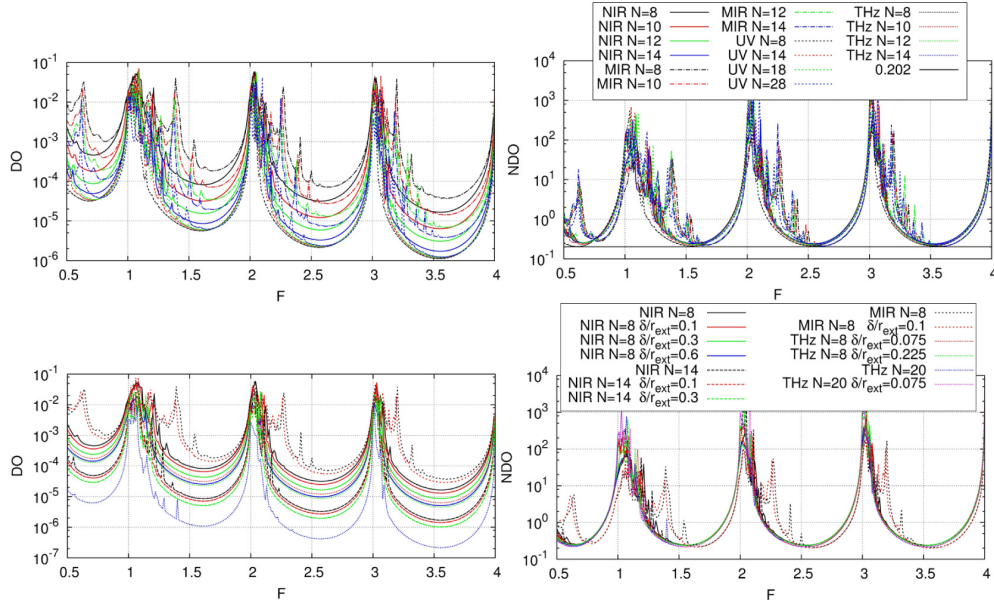


Fig. 9. *DO* (left) and *NDO* (right) of the fibers described in the table and with $\delta = 0$ (top) and $\delta \neq 0$ (bottom).

The following empirical formula is thus able to predict the minimum values of DO over a wide range of wavelength and geometrical dimensions:

$$DO_{min} = \frac{2.4 \cdot 10^{-1}}{n}\left(\frac{\lambda}{R_{co}}\right)^2\left(\frac{t}{R_{co}}\right)^{0.93} = \frac{2.4 \cdot 10^{-1}}{n}\left(\frac{k}{\sin\left(\frac{\pi}{N}\right)} - 1\right)^{-2.93}\left(\frac{t}{r_{ext}}\right)^{0.93}\left(\frac{\lambda}{r_{ext}}\right)^2 . (4)$$

Compared to $CL_{mim}$, $DO_{min}$ exhibits a weaker and simpler dependence on the fiber's parameters. By substituting Eq. (4) in the expression of *AL*, it yields:

$$AL_{min} = 2.4 \cdot 10^{-1}\frac{\alpha_d(\lambda)}{n}\left(\frac{\lambda}{R_{co}}\right)^2\left(\frac{t}{R_{co}}\right)^{0.93} = 2.4 \cdot 10^{-1}\frac{\alpha_d(\lambda)}{n}\left(\frac{k}{\sin\left(\frac{\pi}{N}\right)} - 1\right)^{-2.93}\left(\frac{t}{r_{ext}}\right)^{0.93}\left(\frac{\lambda}{r_{ext}}\right)^2 ,$$

which can be used to estimate the values of the *AL* minima inside the transmission bands.

## 5. Analysis of the EI parameter dependences

Figure 10 shows the *EI* parameter of some fibers considered in the previous analysis and compares it with the normalized coefficient:

$$NEI = EI \cdot \frac{R_{co}^3}{\lambda^2} = EI \left[ \left( k \middle/ \sin\left(\frac{\pi}{N}\right) \right) - 1 \right]^3 \frac{r_{ext}^3}{\lambda^2}.$$
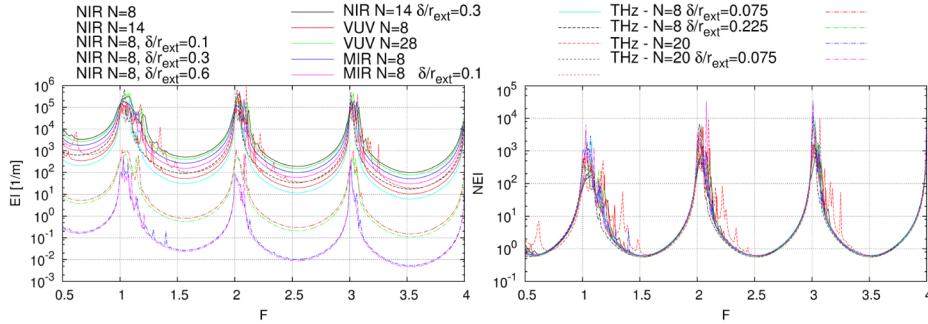


Fig. 10. EI (left) and NEI (right) parameters for some of the fibers described in the table and figure labels.

*EI* ranges over 6 decades, whereas all the minima of *NEI* fall in the range [0.58, 0.67]. By assuming an average value $NEI_{min} = 0.63$, the empirical formula to predict the minima values of *IE* parameter is thus the following:

$$EI_{min} = 0.63 \left( \frac{\lambda}{R_{co}} \right)^2 \frac{1}{R_{co}} = 0.63 \left( \frac{k}{\sin\left(\frac{\pi}{N}\right)} - 1 \right)^{-3} \frac{\lambda^2}{r_{ext}^3}. \tag{5}$$

Conversely to $CL_{min}$ and $DO_{mim}$, $EI_{min}$ does not depend on thickness and refractive index of the tubes composing the cladding. By replacing Eq. (5) in the expression of SSL, it yields:

$$SSL_{min}(\lambda) = 0.63\eta\lambda_0^3 \frac{1}{R_{co}^3} \frac{1}{\lambda}. \tag{6}$$

Equation (6) shows that, conversely to $CL_{min}$, $SSL_{min}$ increases by reducing the wavelength confirming that *SSL* is the main loss mechanism at short wavelength.

## 6. Scaling laws

Compared to other HC fibers, HC-TLFs exhibit stronger *CL* dependence both on $R_{co}$ and on λ. In an air hole surrounded by a uniform infinite dielectric, *CL* scale with $\lambda^2/R_{co}^3$ [23], and in Kagome fibers it scales with $\lambda^3/R_{co}^3$ [24], whereas in HC-TLFs CL scale with $\lambda^{4.5}/R_{co}^4$. Actually the scaling laws in HC-TLFs need a little bit more thorough analysis. In Eqs. (3), (4), and (5) some parameters are not actually degree of freedom: the tube thickness is usually defined by the working wavelength through Eq. (2); the refractive index $n_d$ is defined by the material used, often chosen on the basis of its absorption coefficient, chemical and physical properties, ect. Usually the parameter used to reduce *CL*, *DO*, and *EI*, is the core size. In HC-TLFs $R_{co}$ can be changed by increasing the number of tubes N, their size $r_{ext}$ or their distance δ. All of them affect *CL*, *DO*, and *EI* but in different ways. Figure 11 shows the dependences of $CL_{min}$ on N, k, and $r_{ext}/t$. In the range of reasonable values of N, k, and $n_d$, confinement loss minima scale as $CL_{min} \propto 1/N^\alpha$ with α = 5.1 ÷ 4.8, and k = 1.0 ÷ 1.5; as $CL_{min} \propto 1/k^\alpha$ with α = 5.2 ÷ 4.5, and N = 8 ÷ 20; as $CL_{min} \propto (t/r_{ext})^\alpha$ with α = 6.0 ÷ 6.1, and $n_d$ = 1.44, 2.42.
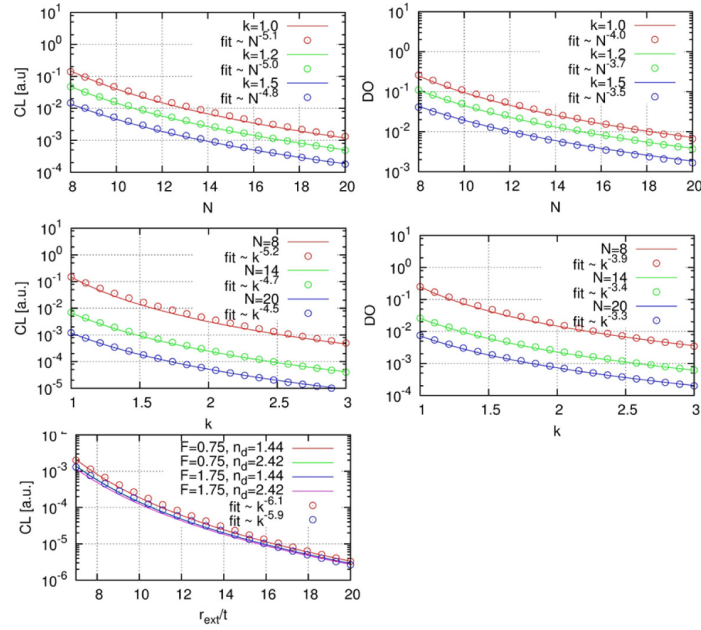
Fig. 11. Trends of CL (left) and DO (right) with respect to number of tubes $N$ (top), tube-tube spacing $k$ (middle), and normalized tube size $r_{ext}/t$ (bottom).

About the wavelength dependence, the effect of the exponential function in Eq. (3) is negligible over the first transmission bands of a given fiber, but it is necessary to take into account the $CL_{min}$ variations which occur passing from a wavelength range to another (i.e. from NIR to MIR or THz). By interpolating the curves of $CL_{min}$ versus $\lambda$, not shown here for sake of brevity, it yields $CL_{min} \propto 1/\lambda^{\alpha}$ with $\alpha = 4.5,\ 4.6$ and $n_d = 1.44,\ 2.42$ respectively. By carry the same analysis out for $DO_{min}$, from Fig. 11 it results $DO_{min} \propto 1/N^{\alpha}$ with $\alpha = 4.0 \div 3.5$, and $k = 1.0,\ 1.5$; $DO_{pmin} \propto 1/k^{\alpha}$ with $\alpha = 3.9 \div 3.3$, and $N = 8 \div 20$. Since the dependences are very similar, the same scaling laws are observed for $EI_{min}$. The results are summarized in the Table 2.

**Table 2. HC-TLFs scaling laws.**

|  | $1/N^{\alpha}$ $(k = 1 \div 1.5)$ | $1/k^{\alpha}(N = 20 \div 8)$ | $(t/r_{ext})^{\alpha}$ | $\lambda^{\alpha}$ |
|---|---|---|---|---|
| $CL_{min}$ | $\alpha = 5.1 \div 4.8$ | $\alpha = 4.5 \div 5.2$ | $\alpha = 6.0 \div 6.1$ | $\alpha = 4.5 \div 4.6$ |
| $DO_{min}$ | $\alpha = 4 \div 3.5$ | $\alpha = 3.3 \div 3.9$ | $\alpha = 2.93$ | $\alpha = 2$ |
| $EI_{min}$ | $\alpha = 4 \div 3.5$ | $\alpha = 3.3 \div 3.9$ | $\alpha = 3$ | $\alpha = 3$ |

## 7. Conclusions

In this paper scaling laws of the confinement loss, dielectric overlap, and electric field at interface of tube lattice fibers with both touching and non-touching tubes have been numerically analyzed. About thirty fibers with different cladding parameters and different working wavelength (from ultraviolet to terahertz band) have been considered. $CL_{min}$ and $DO_{min}$ depend on all fiber's parameter even though $DO$ dependence is weaker than $CL$ one. $EI_{min}$ only depends on the wavelength and core radius, whereas it does not depend on tube thickness and refractive index. Empirical formulas able to predict the minimum values of $CL$, $AL$, and $SSL$ inside the fiber transmission bands have been proposed. These formulas only require the knowledge of the number, dimensions and refractive index of the tubes composing the fiber cladding. They can be useful tools for a quicker and better fiber design and to a better comprehension of the waveguiding and loss mechanisms in HC-TLFs.